Rare Helium-Bearing Compound FeO$_2$He Stabilized at Deep-Earth Conditions

Jurong Zhang,[1] Jian Lv,[1] Hefei Li,[1] Xiaolei Feng,[2,3] Cheng Lu,[4] Simon A. T. Redfern,[2,3]
Hanyu Liu,[1,*] Changfeng Chen,[4,†] and Yanming Ma[1,5,‡]

[1]*State Key Laboratory of Superhard Materials & Innovation Center for Computational Physics Methods and Software,*
College of Physics, Jilin University, Changchun 130012, China
[2]*Center for High Pressure Science and Technology Advanced Research (HPSTAR), Shanghai, 201203, China*
[3]*Department of Earth Sciences, University of Cambridge, Downing Street, Cambridge CB2 3EQ, United Kingdom*
[4]*Department of Physics and Astronomy, University of Nevada, Las Vegas, Nevada 89154, USA*
[5]*International Center of Future Science, Jilin University, Changchun 130012, China*

There is compelling geochemical evidence for primordial helium trapped in Earth's lower mantle, but the origin and nature of the helium source remain elusive due to scarce knowledge on viable helium-bearing compounds that are extremely rare. Here we explore materials physics underlying this prominent challenge. Our structure searches in conjunction with first-principles energetic and thermodynamic calculations uncover a remarkable helium-bearing compound FeO$_2$He at high pressure-temperature conditions relevant to the core-mantle boundary. Calculated sound velocities consistent with seismic data validate FeO$_2$He as a feasible constituent in ultralow velocity zones at the lowermost mantle. These mutually corroborating findings establish the first and hitherto only helium-bearing compound viable at pertinent geophysical conditions, thus providing vital physics mechanisms and materials insights for elucidating the enigmatic helium reservoir in deep Earth.

Helium is the second most abundant element in the Universe and its isotopes provide an important tool for tracing early-Earth, primordial compositions that have survived in the planet's interior [1–3]. It has been long hypothesized that deep mantle harbors domains containing high ratios of primordial ^{3}He to radiogenic ^{4}He produced by radioactive decays of uranium- and thorium-series elements [4–6]. Recent studies of volcanic hot spots have found plumes entrained from Earth's deep mantle hosting high ^{3}He/^{4}He ratios compared to the values identified in mid-ocean-ridge basalts that form by melting the upper mantle [7]. These observations provide compelling evidence for the existence of a deep-mantle reservoir of primordial helium; however, it remains a formidable challenge to explain the origin and nature of this enigmatic helium reservoir. Solving this prominent geoscience puzzle requires advances in understanding the fundamental physics governing the structure and property of viable helium-bearing compounds at high pressure-temperature (P-T) conditions in deep Earth.

The extremely stable closed-shell electron configuration of helium makes it the most unreactive element, and until very recently, there had been no known stable helium-bearing solid compound. Most primordial helium inside the early Earth is expected to have outgassed into the atmosphere and lost to space; however, recent findings of high concentrations of primordial helium in hot plumes entrained from deep mantle point to the existence of yet unknown helium-bearing compounds that have eluded all past studies.

The latest research has identified helium reacting at high P-T conditions with other elements or compounds, such as water [8], sodium and sodium oxide [9], nitrogen [10], and iron [11], but no connections to the deep-Earth helium reservoir have been established. Meanwhile, a theoretical analysis [12] shows that helium tends to react under high pressure with ionic compounds containing an unequal number of cations and anions. A pressing task is to find helium-bearing compounds viable in the deep-mantle P-T and composition environments and compatible with seismic data.

Recent reports [13–18] on high P-T synthesis and characterization of a new iron peroxide FeO$_2$ and its hydrogen-bearing compound suggest their plausible presence in ultralow-velocity zones (ULVZs) that lie directly above Earth's core-mantle boundary (CMB) [19]; these compounds were presumably produced in the lowermost mantle by reaction of iron supplied by the core and water from subducted hydrous minerals. The resulting FeO$_2$ may, following recent analysis [12], react with primordial helium and form a stable compound, thus trapping helium at the lowermost mantle. Motivated by this highly intriguing prospect, we have performed extensive crystal structure searches accompanied by first-principles energetic and thermodynamic calculations, leading to a remarkable computational discovery of a rare FeO$_2$He compound stabilized at the P-T conditions corresponding to CMB. We further carried out *ab initio* molecular dynamics simulations to determine the high P-T elastic parameters and sound

velocities, and the results consistent with seismic data place FeO_2He among viable constituents comprising the enigmatic ULVZs. These findings provide a basis for understanding material compositions and physics mechanisms for the deep-Earth helium reservoir.

The present structure search is based on a global optimization of free-energy surfaces using the CALYPSO methodology [20,21], which has been successfully employed in predicting a large variety of crystal structures [22–30]. Evolutionary variable-cell calculations were performed at 100, 200, and 300 GPa with 1, 2, 3, 4, and 8 FeO_2He formula units (f.u.) per cell, retaining 60% lowest-enthalpy structures to produce the next-generation structures by a particle swarm optimization procedure and generating the remaining 40% structures randomly within the symmetry constraint. Most searches converge in 30 to 40 generations with about 1000 structures generated. First-principles total-energy and electronic property calculations were carried out using the density functional theory (DFT) as implemented in the VASP code [31], adopting the frozen-core all-electron projector-augmented wave (PAW) method [32], with $3s^23p^63d^64s^2$, $2s^22p^4$, and $1s^2$ treated as valence electrons for Fe, O, and He, respectively, and the Perdew-Burke-Ernzerhof (PBE) exchange-correlation functional in the generalized gradient approximation (GGA) [33,34]. Correlation effects among the Fe 3d electrons were treated in the GGA + U approach [35,36], adopting the recently proposed on-site Coulomb interaction U = 5.0 eV and a Hund's coupling $J = 0.8$ eV [15–17,37]. A cutoff energy of 700 eV for the plane-wave expansion and fine Monkhorst-Pack k meshes [38] were chosen to ensure enthalpy convergence of better than 1 meV/atom. Phonon calculations were carried out using a supercell approach [39] as implemented in PHONOPY code [40]. Further computational details are given in the Supplemental Material [41].

Our extensive structure search identifies a rare FeO_2He compound that is stabilized by pressures above 120 GPa. This new helium-bearing compound adopts a cubic structure in Fm-$3m$ symmetry (space group 225, Z = 4), as depicted in Fig. 1(a), with Fe, O, and He occupying the 4b (0.5, 0, 0), 8c (0.75, 0.25, 0.25), and 4a (0, 0, 0) positions. In this structure the He and O atoms build an antifluorite structure while the Fe atoms taking the sites on the top vertex and face of the hexahedron. Each Fe atom is coordinated with eight O atoms and forms a regular hexahedron. Inside its stability pressure range at 135 GPa, Fm-$3m$ FeO_2He has a cubic lattice parameter of a = 4.32 Å, an Fe-O bond length of ~1.87 Å, and an O-Fe-O angle of 70.53°. Calculated enthalpy results in Fig. 1(b) show that Fm-$3m$ FeO_2He quickly becomes energetically favorable at rising pressures beyond 120 GPa compared to the decomposition products Pa-3-FeO_2 [13,15] and hcp He [42,43], and the steep enthalpy decrease indicates strong stability of this newly formed compound. We also constructed the convex hull, and the
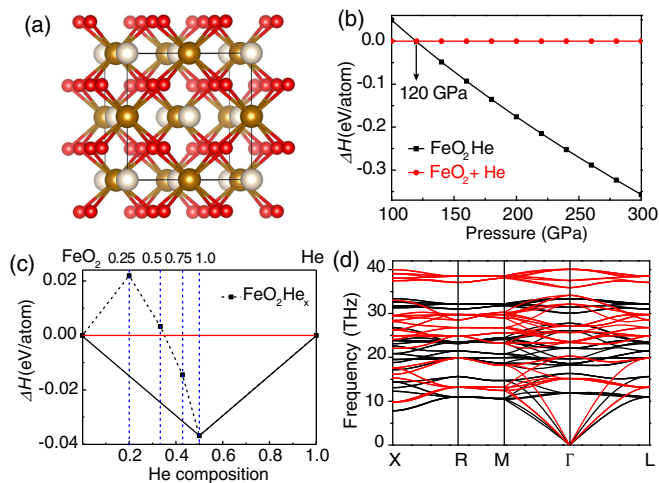

FIG. 1. (a) Crystal structure of the predicted Fm-$3m$ FeO_2He, where the golden, red, and white spheres represent Fe, O, and He atoms, respectively. (b) Calculated formation enthalpy of Fm-$3m$ FeO_2He relative to decomposition products FeO_2 + He as a function of pressure at 0 K. (c) The convex hull (black solid lines) of the $FeO_2 - He$ system at 135 GPa, where the enthalpy values for structures with partial He content FeO_2He_x with $x < 1$, as indicated by the numbers at the top of the panel, are connected by black dashed lines. (d) Calculated phonon dispersion of Fm-$3m$ FeO_2He at 135 (black lines) and 300 GPa (red lines).

results at 135 GPa shown in Fig. 1(c) indicate that compounds with partial He content, FeO_2He_x ($x = 0.25$, 0.5, 0.75), are unstable against decomposition into Fm-$3m$ FeO_2He and Pa-$3FeO_2$, which would form a solid solution in a helium relatively deficient environment. This result is consistent with the large enthalpy differences between Fm-$3m$ FeO_2He and its decomposition products seen in Fig. 1(b), and the same trend is expected in the entire pressure range where the FeO_2He phase is stable. Our phonon calculations have found no imaginary modes in the pressure range from 120 and 300 GPa [results at 135 and 300 GPa are shown in Fig. 1(d)], confirming robust dynamic stability of Fm-$3m$ FeO_2He.

To assess the viability of Fm-$3m$ FeO_2He in the deep mantle environment, we further examine its structural stability at relevant simultaneous high P-T conditions. To this end, we have performed two sets of calculations. First, we calculated volume-dependent phonon dispersions and the corresponding phonon density of states (PDOS) using the quasi-harmonic approximation as implemented in PHONOPY code [40], and used the obtained PDOS as input to evaluate the vibrational contribution to the entropy of each phase. The results are combined with the total internal energy, pressure and volume obtained from the VASP calculations to compute the Gibbs free energies of the relevant phases. Relative Gibbs free energies of Fm-$3m$ FeO_2He and the decomposition products FeO_2 and He determine the P-T phase diagram presented in Fig. 2(a). The stability field of Fm-$3m$ FeO_2He shifts toward higher
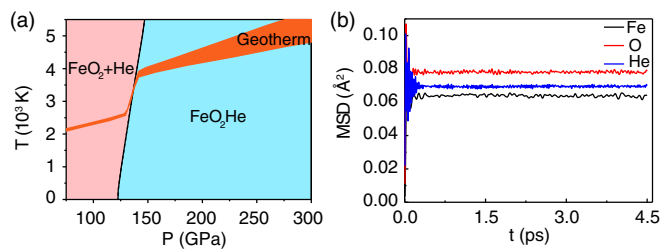
FIG. 2. (a) Pressure-temperature (P-T) phase diagram showing the stability field of Fm-$3m$ FeO$_2$He and its boundary with the decomposition products FeO$_2$ + He. Also shown is the geotherm indicating the P-T profile in Earth's interior. (b) Calculated mean-square-deviation (MSD) of the atomic positions of Fm-$3m$ FeO$_2$He at 135 GPa and 3000 K.

FIG. 3. Electronic band structures (left) and density of states (DOS) (right) of Fm-$3m$ FeO$_2$He at indicated pressures.

pressures as temperature rises, and the phase boundary interests with Earth's geotherm [44] at $P = 135$ GPa and $T = 3000$ K, which corresponds to the CMB region. This remarkable result places FeO$_2$He at the lowermost mantle, where both reactants, i.e., FeO$_2$ and primordial helium, have been identified by recent studies [7,13,15], thus making all pertinent results consistent and mutually corroborating. In a second set of calculations, we employed *ab initio* molecular dynamics (AIMD) simulations [45] to directly assess the structural integrity of the FeO$_2$He crystal at the identified P-T condition of 135 GPa and 3000 K. The obtained mean-square-deviations (MSD) of atomic positions are shown in Fig. 2(b), and it is seen that the Fe, O, and He atoms all remain on their lattice sites, offering compelling evidence for the structural stability of Fm-$3m$ FeO$_2$He at the CMB P-T conditions.

We also characterized Fm-$3m$ FeO$_2$He by examining its charge distribution, bonding character, and electronic band structure. We calculated the Bader charge in the FeO$_2$He structure at 135 GPa using the quantum theory of atoms-in-molecules approach [46]. The obtained results reveal that the O atoms gain 0.80 e^- per atom, Fe atoms donate 1.64 e^- per atom, and He atoms gain 0.04 e^- per atom. These data show that there is little charge transfer between the FeO$_2$ and He units, indicating that the He atoms mainly serve as a Coulomb shield in stabilizing the compound, which is consistent with recent theoretical analysis on similar materials [12]. Electronic band structure calculations show that FeO$_2$He is a semiconductor with an indirect gap (Fig. 3) of the size 0.95 eV at 135 GPa. The valence-band maximum and conduction-band minimum are located at Γ and R points, respectively. Moreover, the band gap of FeO$_2$He increases slightly with rising pressure.

The newly identified FeO$_2$He compound has major implications for another prominent topic in geoscience, namely, the composition of ULVZs that host anomalous variations of density and seismic wave speeds compared to the preliminary reference Earth model (PREM) [47]. The origin of these anomalous phenomena has been long debated, and seismological studies have revealed that
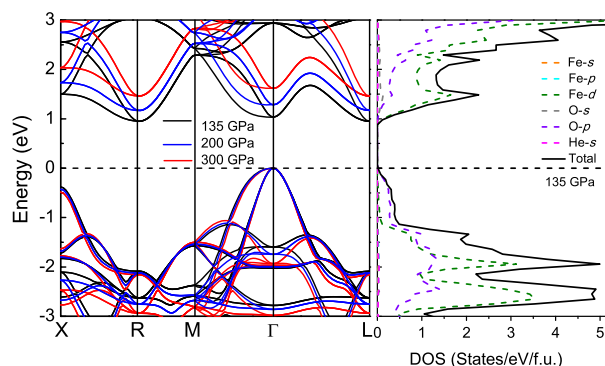
ULVZs comprise dense domains where the density is increased by about 10% and seismic wave speeds are depressed by about 10% for P waves (V_P) and by about 10% to 30% for S waves (V_S) relative to the PREM [48–50]. Previous studies [50–55] have attributed ULVZs to either partial melting that results in a molten region with a significantly reduced shear modulus or chemical inhomogeneity with iron enriched constituents such as (Mg, Fe) O [56,57] or FeOOH$_x$ [15] producing the enhanced density and depressed seismic wave speeds. Meanwhile, there also exist alternative proposed mechanisms for ULVZs involving other compounds, such as accumulated silicate sediments from the core [58], subducted banded iron formations [59], iron-enriched mantle phases like postperovskite [60] and ferropericlase [56], and iron-carbon metallic melts forming in the lowermost mantle [61]. These studies suggest that there may be multiple types of densified regions near the CMB generating ULVZs with a diverse variety of compositions. Here we examine FeO$_2$He as a feasible candidate material for ULVZs to advance the knowledge on compositional, chemical, and physical characteristics of the CMB region.

We compute sound velocities of FeO$_2$He at the CMB P-T conditions and compare the results with seismic data. The elastic responses for the FeO$_2$He crystal were simulated using an AIMD-based strain-stress method [62]. The resulting stress tensors were used to determine the elastic-wave velocities by solving the Cristoffel equation, defined as det $|T_{ik} - \delta_{ik}\rho V^2| = 0$, where δ_{ik} is the Kronecker delta function, V is one of the seismic velocities, and T_{ik} is the Christoffel stiffness [65]. From these calculations, we have obtained key properties of FeO$_2$He at 135 GPa and 3000 K, including its density of 7.226 g/cm^3, which lies within the range of ULVZs (5.57–8.91 g/cm^3) [48] and its mean seismic wave speeds V_P and V_S of 11.52 and 6.14 km/s, respectively. These velocities represent reductions of 16.05% and 15.42%, respectively, relative to the PREM values at the CMB region, which are fully consistent with the constraints imposed by the seismic data, making FeO$_2$He a viable constituent in ULVZs. We also have
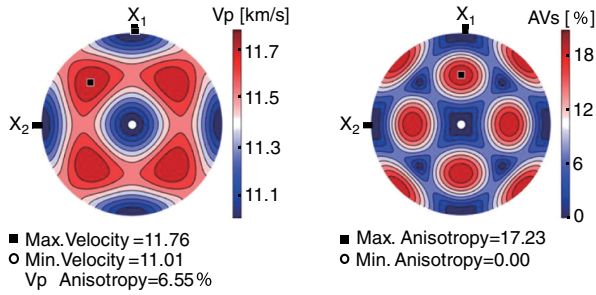
FIG. 4. Stereographic projections of the calculated P-wave velocity V_P (in km/s) and S-wave anisotropy AV_S (in %) for Fm-$3m$ FeO$_2$He at 135 GPa and 3000 K. The coordinate axes are $X_1 = [100]$, $X_2 = [010]$, $X_3 = [001]$. The black square and white circle in each plot indicate the crystallographic directions of the maximum and minimum values, respectively.

assessed the directional propagation of sound waves by examining their anisotropy $AV_X = 100\% \times (V_{X\,\text{max}} - V_{X\,\text{min}})/[(V_{X\,\text{max}} + V_{X\,\text{min}})/2]$ ($X = P,\ S$). The obtained sound-velocity profiles at 135 GPa and 3000 K shown in Fig. 4 reveal the distribution in different crystallographic directions [65,66]. The extremal P-wave propagations of FeO$_2$He occur in the basal plane, with the fastest velocity ($V_{P\,\text{max}} = 11.76$ km/s) along the [221] direction and the slowest ($V_{P\,\text{min}} = 11.01$ km/s) along the [001] direction. The corresponding AV_P and AV_S are 6.55% and 17.23%, respectively, which indicate a moderate degree of anisotropy that may exist within a texture-developing stress field within an ULVZ. While FeO$_2$He may represent only a small fraction of the total matter at the CMB zone, our results indicate that this new compound conforms to the constraints imposed by the seismic data and may contribute to lowering the velocities of seismic waves.

In this work we also explored possibilities of helium forming stable compounds with other typical deep-Earth constituents, e.g., MgO, MgSiO$_3$, and Fe in the relevant pressure range from 100 to 300 GPa. However, our systematic searches found no such stable compounds, which is consistent with previously reported findings [11,53,54], and these results highlight the crucial role of FeO$_2$ in trapping helium at the base of the lower mantle. In light of the strong geochemical evidence for a lower-mantle helium reservoir, the prominent helium-trapping ability of FeO$_2$ serves as a powerful corroborating evidence for its presence near the CMB as suggested by newly reported experimental and theoretical discoveries [14–16]. Recent studies indicate that FeO$_2$ may form solid solutions with select minerals at the lowermost mantle [15], raising prospects that such solid solutions may also possess helium-trapping capacity. Pertinent FeO$_2$-derived multi-component helium-bearing constituents near the CMB warrant further research.

While the present work provides strong theoretical evidence for reaction of FeO$_2$ and ^{3}He at deep-Earth conditions, thereby creating a helium reservoir at the CMB zone, a key question on why He was not evacuated in stages prior to the formation of the definitive structure of the Earth remains open and requires further research. A couple of alternative mechanisms for the existence of ^{3}He ejected in the mid-ocean ridge and in the volcanic hot spots have been considered but deemed unlikely, including spallation reactions, which would require too much energy, and reaction between neutrinos and ^{4}He, which has too small a cross section to generate the observed quantity.

In summary, our crystal structure searches combined with property calculations have identified a rare helium-bearing compound FeO$_2$He stabilized at high P-T conditions relevant to the CMB. A systematic examination of key physical properties reveals that the density and compressional and shear sound speeds of FeO$_2$He are well consistent with the seismic data, thus validating this newly uncovered compound as a viable constituent in ULVZs. The present results put forth a compelling scenario for helium trapped at the lowermost mantle by reacting with FeO$_2$ whose presence in the CMB region has been substantiated by recent independent studies. These mutually corroborating findings establish robust material sources and physics mechanisms for unraveling the origin and nature of the enigmatic deep-Earth primordial helium reservoir inferred from geochemical observations. The present work also sets the stage for further exploration of related materials physics issues in this very active multidisciplinary research field.

[*]hanyuliu@jlu.edu.cn
[†]chen@physics.unlv.edu
[‡]mym@jlu.edu.cn

[1] S. Mukhopadhyay, Nature (London) **486**, 101 (2012).
[2] H. Rizol, R. J. Walker, R. W. Carlson, M. F. Horan, S. Mukhopadhyay, V. Manthos, D. Francis, and M. G. Jackson, Science **352**, 809 (2016).
[3] M. G. Jackson, R. W. Carlson, M. D. Kurz, P. D. Kempton, D. Francis, and J. Blusztajn, Nature (London) **466**, 853 (2010).
[4] C. J. Allègre, T. Staudacher, P. Sarda, and M. D. Kurz, Nature (London) **303**, 762 (1983).

[5] S. R. Hart, E. H. Hauri, L. A. Oschmann, and J. A. Whitehead, Science **256,** 517 (1992).

[6] C. Class and S. L. Goldstein, Nature (London) **436,** 1107 (2005).

[7] M. G. Jackson, J. G. Konter, and T. W. Becker, Nature (London) **542,** 340 (2017).

[8] H. Liu, Y. Yao, and D. D. Klug, Phys. Rev. B **91,** 014102 (2015).

[9] X. Dong, A. R. Oganov, A. F. Goncharov, E. Stavrou, S. Lobanov, G. Saleh, G. R. Qian, Q. Zhu, C. Gatti, V. L. Deringer, R. Dronskowski, X. F. Zhou, V. B. Prakapenka, Z. Konopkova, I. A. Popov, A. I. Boldyrev, and H. T. Wang, Nat. Chem. **9,** 440 (2017).

[10] Y. Li, X. Feng, H. Liu, J. Hao, S. A. T. Redfern, W. Lei, D. Liu, and Y. Ma, Nat. Commun. **9,** 722 (2018).

[11] B. Monserrat, M. Martinez-Canales, R. J. Needs, and C. J. Pickard, Phys. Rev. Lett. **121,** 015301 (2018).

[12] Z. Liu, J. Botana, A. Hermann, S. Valdez, E. Zurek, D. Yan, H. Q. Lin, and M. S. Miao, Nat. Commun. **9,** 951 (2018).

[13] Q. Hu, D. Y. Kim, W. G. Yang, L. X. Yang, Y. Meng, L. Zhang, and H. K. Mao, Nature (London) **534,** 241 (2016).

[14] M. Nishi, Y. Kuwayama, J. Tsuchiya, and T. Tsuchiya, Nature (London) **547,** 205 (2017).

[15] J. Liu, Q. Y. Hu, D. Y. Kim, Z. Q. Wu, W. Z. Wang, Y. M. Xiao, P. Chow, Y. Meng, V. B. Prakapenka, H. K. Mao, and W. L. Mao, Nature (London) **551,** 494 (2017).

[16] C. Lu and C. F. Chen, J. Phys. Chem. Lett. **9,** 2181 (2018).

[17] C. Lu, M. Amsler, and C. F. Chen, Phys. Rev. B **98,** 054102 (2018).

[18] G. L. Weerasinghe, C. J. Pickard, and R. J. Needs, J. Phys. Condens. Matter **27,** 455501 (2015).

[19] J. W. Hernlund, *Deep Earth: Physics and Chemistry of the Lower Mantle and Core* (American Geophysical Union, Washington, DC, 2016), p. 201.

[20] Y. C. Wang, J. Lv, L. Zhu, and Y. M. Ma, Phys. Rev. B **82,** 094116 (2010).

[21] Y. C. Wang, J. Lv, L. Zhu, and Y. M. Ma, Comput. Phys. Commun. **183,** 2063 (2012).

[22] J. Lv, Y. C. Wang, L. Zhu, and Y. M. Ma, Phys. Rev. Lett. **106,** 015503 (2011).

[23] L. Zhu, H. Wang, Y. C. Wang, J. Lv, Y. M. Ma, Q. L. Cui, Y. M. Ma, and G. T. Zou, Phys. Rev. Lett. **106,** 145501 (2011).

[24] L. Zhu, H. Y. Liu, C. J. Pickard, G. T. Zou, and Y. M. Ma, Nat. Chem. **6,** 644 (2014).

[25] D. Zhou, Q. Li, Y. M. Ma, Q. L. Cui, and C. F. Chen, J. Phys. Chem. C **117,** 5352 (2013).

[26] Q. Li, D. Zhou, W. T. Zheng, Y. M. Ma, and C. F. Chen, Phys. Rev. Lett. **110,** 136403 (2013).

[27] M. Zhang, H. Y. Liu, Q. Li, B. Gao, Y. C. Wang, H. D. Li, C. F. Chen, and Y. M. Ma, Phys. Rev. Lett. **114,** 015502 (2015).

[28] Q. Li, D. Zhou, W. T. Zheng, Y. M. Ma, and C. F. Chen, Phys. Rev. Lett. **115,** 185502 (2015).

[29] D. Zhou, Q. Li, W. T. Zheng, Y. M. Ma, and C. F. Chen, Phys. Chem. Chem. Phys. **19,** 4560 (2017).

[30] C. Lu, Q. Li, Y. M. Ma, and C. F. Chen, Phys. Rev. Lett. **119,** 115503 (2017).

[31] G. Kresse and J. Furthmüller, Phys. Rev. B **54,** 11169 (1996).

[32] P. E. Blöchl, Phys. Rev. B **50,** 17953 (1994).

[33] J. P. Perdew and Y. Wang, Phys. Rev. B **45,** 13244 (1992).

[34] J. P. Perdew, K. Burke, and M. Ernzerhof, Phys. Rev. Lett. **77,** 3865 (1996).

[35] V. I. Anisimov, I. V. Solovyev, M. A. Korotin, M. T. Czyżyk, and G. A. Sawatzky, Phys. Rev. B **48,** 16929 (1993).

[36] L. Wang, T. Maxisch, and G. Ceder, Phys. Rev. B **73,** 195107 (2006).

[37] Q. Hu, D. Y. Kim, J. Liu, Y. Meng, L. Yang, D. Zhang, W. L. Mao, and H.-K. Mao, Proc. Natl. Acad. Sci. U.S.A. **114,** 1498 (2017).

[38] H. J. Monkhorst and J. D. Pack, Phys. Rev. B **13,** 5188 (1976).

[39] K. Parlinski, Z. Q. Li, and Y. Kawazoe, Phys. Rev. Lett. **78,** 4063 (1997).

[40] A. Togo, F. Oba, and I. Tanaka, Phys. Rev. B **78,** 134106 (2008).

[41] See Supplemental Material at http://link.aps.org/supplemental/10.1103/PhysRevLett.121.255703 for details onk-mesh convergence check for the electronic density of states calculations and the mesh choice for the Bader analysis, and the structure of FeO_2 at 135 GPa in CIF format.

[42] P. Loubeyre, R. LeToullec, J. P. Pinceaux, H. K. Mao, J. Hu, and R. J. Hemley, Phys. Rev. Lett. **71,** 2272 (1993).

[43] B. Monserrat, N. D. Drummond, C. J. Pickard, and R. J. Needs, Phys. Rev. Lett. **112,** 055504 (2014).

[44] S. Anzellini, A. Dewaele, M. Mezouar, P. Loubeyre, and G. Morard, Science **340,** 464 (2013).

[45] We have performed AIMD simulations using the VASP code for the FeO_2He crystal at 135 GPa and 3000 K. A $2 \times 2 \times 2$ supercell containing 128 atoms and a cutoff energy of 700 eV were adopted. To calculate the mean-square-deviation (MSD) of atomic positions, we adopted an NPT ensemble, and each simulation was run for 10 ps with a time step of 1 fs. Data from the first half of the run were discarded and those from the second half were used to compute the MSD defined by $(1/N) \sum_i \langle [r_i(t) - r_i(0)]^2 \rangle$, where N is the total number of atoms, $r_i(t)$ and $r_i(0)$ are, respectively, the positions of the ith atom at time t and initial moment ($t = 0$), and $\langle \dots \rangle$ indicates an ensemble average.

[46] R. F. W. Bader, *Atoms in Molecules: A Quantum Theory* (Oxford University Press, Oxford, 1994).

[47] A. M. Dziewonski and D. L. Anderson, Phys. Earth Planet. Inter. **25,** 297 (1981).

[48] M. S. Thorne and E. J. Garnero, J. Geophys. Res. **109,** B08301 (2004).

[49] E. J. Garnero and D. V. Helmberger, Geophys. Res. Lett. **23,** 977 (1996).

[50] A. K. McNamara, E. J. Garnero, and S. Rost, Earth Planet. Sci. Lett. **299,** 1 (2010).

[51] S. Ni and D. V. Helmberger, Geophys. Res. Lett. **28,** 2345 (2001).

[52] L. Wen and D. V. Helmberger, Science **279,** 1701 (1998).

[53] Q. Williams and E. J. Garnero, Science **273,** 1528 (1996).

[54] S. Anzellini, A. Dewaele, M. Mezouar, P. Loubeyre, and G. Morard, Science **340,** 464 (2013).

[55] M. S. Thorne, E. J. Garnero, G. Jahnke, H. Igel, and A. K. McNamara, Earth Planet. Sci. Lett. **364,** 59 (2013).

[56] J. K. Wicks, J. M. Jackson, and W. Sturhahn, Geophys. Res. Lett. **37,** L15304 (2010).

[57] W. L. Mao, H. K. Mao, W. Sturhahn, J. Y. Zhao, V. B. Prakapenka, Y. Meng, J. F. Shu, Y. W. Fei, and R. J. Hemley, Science **312,** 564 (2006).

[58] B. A. Buffett, E. J. Garnero, and R. Jeanloz, Science **290,** 1338 (2000).

[59] D. P. Dobson and J. P. Brodholt, Nature (London) **434,** 371 (2005).

[60] W. L. Mao, H. K. Mao, W. Sturhahn, J. Zhao, V. B. Prakapenka, Y. Meng, J. F. Shu, Y. Fei, and R. J. Hemley, Science **312,** 564 (2006).

[61] J. Liu, J. Li, R. Hrubiak, and J. S. Smith, Proc. Natl. Acad. Sci. U.S.A. **113,** 5547 (2016).

[62] We ran AIMD simulations following the same procedure described above [45], but adopted an NVT ensemble. Each simulation was run for 4 ps, and the structural data obtained from the second half of the run were taken as input to compute the elastic parameters using the strain-stress method [63,64].

[63] Y. Le Page and P. Saxe, Phys. Rev. B **65,** 104104 (2002).

[64] L. V. B. Martorell, J. Brodholt, and I. G. Wood, Science **342,** 466 (2013).

[65] D. Mainprice, Comput. Geosci. **16,** 385 (1990).

[66] B. Ko and H. Jung, Nat. Commun. **6,** 6586 (2015).